Available online at www.sciencedirect.com
ScienceDirect
C. R. Physique 8 (2007) 745–762
COMPTES RENDUS PHYSIQUE
http://france.elsevier.com/direct/COMREN/

Neutron scattering/Diffusion de neutrons

Inelastic neutron scattering study of spin excitations in the superconducting state of high temperature superconductors

Yvan Sidis [a,*], Stéphane Pailhès [a], Vladimir Hinkov [b], Benoît Fauqué [a], Clemens Ulrich [b], Lucia Capogna [c], Alexandre Ivanov [c], Louis-Pierre Regnault [d], Bernhard Keimer [b], Philippe Bourges [a]

[a] *Laboratoire Léon-Brillouin, CEA–CNRS, CE-Saclay, 91191 Gif sur Yvette, France*
[b] *Max-Planck-Institut für Fertkörperforschung, 70569 Stuttgart, Germany*
[c] *Institut Laue-Langevin, 156X, 38042 Grenoble cedex 9, France*
[d] *CEA Grenoble, DRFMC 38054 Grenoble cedex 9, France*

Available online 23 October 2007

Abstract

Inelastic neutron scattering is a powerful technique that can measure magnetic correlations in a large momentum and energy range. In strongly correlated electronic systems, where spin, orbital, lattice and charge degrees of freedom are entangled, it is currently used to study the magnetic properties and shed light on their role in the appearance of the exotic electronic properties, such as unconventional superconductivity. In this article, we focus on the observation by inelastic neutron scattering technique of unconventional spin triplet collective modes in the superconducting state of high temperature superconducting cuprates and its interplay with anomalies in the charge excitation spectrum. The triplet spin mode is interpreted as a *spin exciton*, within a spin band model. Alternative scenarii based on localized or dual (itinerant localized) models are also mentioned. ***To cite this article: Y. Sidis et al., C. R. Physique 8 (2007).***

Résumé

Étude par diffusion inélastique de neutrons des excitations de spin dans la phase supraconductrice des supraconducteurs à haute température. La diffusion inélastique de neutrons est une technique très efficace qui permet de mesurer les corrélations magnétiques sur une large gamme de vecteurs d'onde et d'énergies. Dans le cadre de l'étude des systèmes d'électrons fortement corrélés, pour lesquels les degrés de liberté des spins, des orbitales, du réseau et des charges sont fortement couplés, cette technique est couramment utilisée pour sonder les propriétés magnétiques et tester leur rôle dans l'établissement de propriétés électroniques exotiques, telles que la supraconductivité non conventionnelle. Dans cet article, nous nous focalisons sur l'observation par diffusion inélastique de neutrons d'un mode d'excitation de spin triplet inhabituel dans la phase supraconductrice des cuprates supraconducteurs à haute température critique, ainsi qu'à son implication dans l'apparition d'anomalies dans le spectre d'excitations des charges. Ce mode est interprété comme un *exciton de spin* sur la base d'une description itinérante des excitations magnétiques. D'autres interprétations en termes de spins localisés ou impliquant une description mixte itinérante-localisée seront également présentées. ***Pour citer cet article : Y. Sidis et al., C. R. Physique 8 (2007).***

* Corresponding author.
E-mail address: yvan.sidis@cea.fr (Y. Sidis).

1631-0705/$ – see front matter
doi:10.1016/j.crhy.2007.07.003

Keywords: Inelastic neutron scattering; Spin dynamics; High temperature superconductivity

Mots-clés : Diffusion inélastique de neutrons ; Dynamique de spins ; Supraconductivité à haute température

1. Introduction

High temperature superconducting copper oxide systems are layered perovskite materials characterized by the stacking of CuO_2 planes [1]. There can be one or several CuO_2 planes per unit cell. These planes are separated by other atomic layers that play the role of charge reservoirs. By transferring charges between the charge reservoirs and the CuO_2 planes, the CuO_2 planes can be doped either with electrons or holes. The charge transfer can be achieved by ionic substitution, such as in $La_{2-x}Sr_xCuO_4$, or by modification of the oxygen stoichiometry, such as in $YBa_2Cu_3O_{6+x}$. The generic phase diagram of electron-doped and hole-doped high temperature superconducting copper oxides is reported in Fig. 1 [2,3]. At zero doping, there is one electron located in $3d_{x^2-y^2}$ orbital on each Cu^{2+} ion. In term of band structure, one could expect a half filled band and therefore the system should be a good metal. On the contrary (Fig. 1), these materials are insulators at very high temperature and on cooling exhibit an antiferromagnetic (AF) order, between 300 K and 400 K depending on each cuprate family. This AF order is well described by the Heisenberg model applied to localized quantum spins $S = 1/2$ on copper sites. The fact that the system is an insulator well above the Néel temperature indicates that there is a large on-site Coulomb repulsion U_d on Cu sites that prohibits the double occupancy. Upon doping, the AF order is destroyed, and the system undergoes a transition from the insulating state to the superconducting state. As a function of doping, the superconducting critical temperature first increases, reaches a maximum at a doping level $\sim$16% and then further decreases [4]. The doping level at which T_c is maximum is called optimal doping and one usually defines two sub-regimes on both sides of the optimal doping: the underdoped regime where T_c increases with increasing doping and the overdoped regime where T_c decreases at higher doping. In the phase diagram as a function of temperature and hole (or electron) doping (Fig. 1), the superconducting critical temperature exhibits a characteristic dome-like shape centered at optimal doping.

The superconductivity in high temperature superconductors is unconventional. This is not only due to the exceptionally large T_c that can be obtained in these materials and that can be as high as 130 K (or even 160 K under pressure) in hole doped systems. This is also due to the symmetry of the superconducting order parameter. As in conventional superconductors, superconductivity implies the formation of pairs of electrons (the Cooper pairs) and these pairs acquire a phase coherence at T_c. In conventional superconductors, the Cooper pairs are in a s-wave singlet spin state. The superconducting order parameter is isotropic. At variance, in superconducting cuprates it is now well established that the superconducting order parameter is anisotropic: Cooper pairs are in a d-wave spin singlet state [5]. The superconductor order parameter can therefore change sign and exhibits nodes along the diagonal directions.

In the rest of the article, we are going to focus on the case of hole doped cuprates which display the highest superconducting critical temperature (T_c) and have been the most studied by inelastic neutron scattering (INS). Before

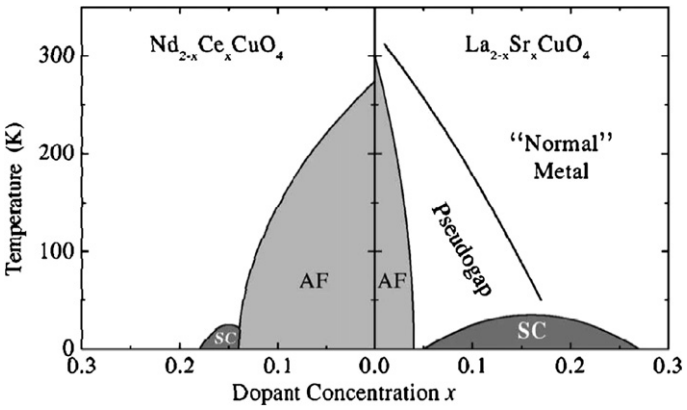

Fig. 1. Generic phase diagram of hole doped (right panel) and electron doped (left panel) high temperature superconducting cuprates [2,3]. The phase diagram shows different states: the antiferromagnetic state (AF) and the d-wave superconducting state (SC).

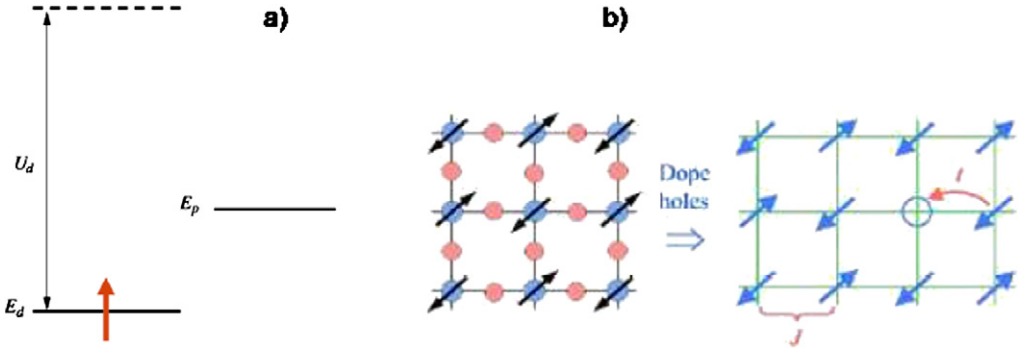

Fig. 2. (a) Electronic structure of a CuO_2 plaquette. (b) Schematic description of the CuO_2 plane (Cu^{2+} ions in blue, O^{2-} ions in red). The solid lines stand for the Cu–O bonds and the black arrows for the spin $S = 1/2$ on a copper site. J indicates the antiferromagnetic super-exchange interaction between nearest neighbour Cu spins. The CuO_2 plane can be viewed as a square lattice made of CuO_2 plaquettes, characterized by 3 different states: $|\uparrow\rangle$ or $|\downarrow\rangle$, when there is no doped hole on the plaquette and $|0\rangle$ when there is a doped hole (Zhang–Rice singlet). The hopping of a doped hole induces a distortion of the AF correlation. The figure is reproduced from Ref. [3].

discussing the magnetic properties of cuprates, it is interesting to consider their electronic structure (here, we follow the description given in Ref. [3] by P.A. Lee et al.). There is now a consensus that the exotic electronic properties of cuprates occur in CuO_2 planes. As mentioned above, the large on-site Coulomb repulsion on copper U_d splits the Cu $3d_{x^2-y^2}$ electronic level: E_d and $E_d + U_d$ (Fig. 2(a)). The O $2p$ electronic level is located at an energy E_p, above E_d (Fig. 2(a)). At zero doping, there is one hole on the Cu $3d$ shell at E_d and it can virtually hop on the oxygen, yielding a superexchange antiferromagnetic interaction between $S = 1/2$ spins on copper sites. Once the system is doped with holes, there are two crucial questions to answer: what is the minimum Hamiltonian to deal with properties of cuprates? What is the effect of the motion of a doped hole in an antiferromagnetically correlated media? The physics of the CuO_2 planes is described by a three band Hubbard model, which is extremely difficult to handle theoretically. A large majority of theoretical models considers that the low energy properties of cuprates can be captured using an effective one-band Hubbard model on a squared lattice:

$$H = -\sum_{\langle i,j\rangle,\sigma} t_{i,j} c^+_{i,\sigma} c_{j,\sigma} + U \sum_i n_{i,\uparrow} n_{i,\downarrow} \tag{1}$$

Here $c^+_{i,\sigma}$ is the usual fermion creation operator on site i and $n_i = \sum_\sigma c^+_{i,\sigma} c_{i,\sigma}$ the number operator. In particular, it was shown by Zhang and Rice [6] that a doped hole on an oxygen site can form a singlet state with an electron on a neighboring Cu site. The Zhang–Rice singlet can hop from one Cu site to another. Since this hopping is a two step process, the effective hoping integral t is of the order of $t_{pd}/(E_p - E_d)$, where t_{pd} is the hopping integral between the oxygen and the copper. Then, the three band Hubbard model can be simplified to a one-band model on a square lattice with an effective hopping integral t and an effective on-site Coulomb repulsion $U = E_p - E_d$. In the large U $(= E_p - E_d)$ limit, this maps onto the t–J model:

$$H = P\left[-\sum_{\langle i,j\rangle,\sigma} t_{i,j} c^+_{i,\sigma} c_{j,\sigma} + \sum_{\langle i,j\rangle} J_{i,j}\left(S_i S_j - \frac{1}{4} n_i n_j\right)\right] P \tag{2}$$

P is the projection operator that excludes the double occupancy on each site. J is the superexchange interaction $\frac{4t^2}{U} \sim \frac{4t_{pd}^4}{(E_d - E_p)^3}$. Note that at half filling, the t–J model reduces to the Heisenberg Hamiltonian. Furthermore, as shown in Fig. 2(b), the hopping of the Zhang–Rice singlet induces a flip of the spin. That is the reason why the motion of doped holes quickly destroys the AF order. Furthermore, in the presence of strong AF correlations, the motion of charge and spin fluctuations have to be bound together. Finally, it has also been emphasized that apical oxygens and the Cu $4s$ orbital can also contribute to additional hopping integrals along the diagonal t' and on next-nearest neighbours t''. The introduction of t' and t'' breaks the electron–hole symmetry and can explain why the phase diagram is not symmetric with respect to electron and hole dopings (Fig. 1).

These Hamiltonians are purely *electronic*, the coupling of the electrons with the lattice is ignored. In conventional superconductors, the superconducting pairing is mediated by the exchange of phonons: owing to the *electron–phonon*

coupling, an electron generates a virtual phonon which is absorbed by a second electron. This gives rise to an effective attractive interaction between electrons responsible for the superconducting pairing. The sensitivity of the superconducting temperature to isotopic substitution, that modifies the frequency of the phonons, is one experimental observation that supports the predominant role of the *electron–phonon* coupling in the superconducting pairing mechanism in conventional superconductors. In high temperature superconductors, the d-wave symmetry of the superconducting order parameter, on the one hand, and the absence of a significant isotopic effect, on the other hand, question the leading role of the *electron–phonon* coupling as a driving force leading the superconducting pairing. At variance, soon after the discovery of superconductivity at high temperature, it has been proposed that a purely electronic mechanism could be at the origin of superconductivity and could involve antiferromagnetic properties of these materials [7,8]. Using a one-band Hubbard model to describe the low energy physics of cuprates, one can find two limits [9]: (a) the strong coupling limit where U is much larger than the band width ($W = 8t$); (b) the weak coupling limit where U is smaller than the band width [7]. For sake of simplicity, one can say that in the strong coupling limit the Hubbard model maps onto the t–J and $J(q) = 2(\cos(q_x) - \cos(q_y))$ may play the role of a direct attractive interaction for the d-wave superconducting pairing. In the weak coupling limit, the pairing interaction is mediated by the exchange of spin fluctuations and the pair potential responsible for the superconducting pairing is found to be proportional to $\sim U^2\chi(\mathbf{q}, \omega)$, which can be viewed as the on-site Coulomb repulsion dressed by magnetic fluctuations. $\chi(\mathbf{q}, \omega)$ is the generalized spin susceptibility [8]. In both cases, U is essential, as it is repulsive on a given site, but contributes to generate AF interaction or AF correlations which makes the particle–particle interaction attractive on the nearest neighbor sites, leading to d-wave superconductivity. One usually considers that the typical orders of magnitude are: $U \sim 2$ eV, $t \sim 0.3$ eV, yielding a J value of about 0.13 eV, in agreement with the experimental value deduced from two-magnon Raman scattering measurements [11] and the study of spin waves by inelastic neutron scattering in the insulating AF state (see Refs. [12,13]). Note, that with these values, the system should be in an intermediate regime between strong and weak coupling ($U \sim W$). For further details, the different theoretical models for superconducting pairing approaches based on magnetic properties of cuprates are summarized in Ref. [10] and also compared to other theories of high temperature superconductivity, based on phonons, for instance.

To summarize the complexity of these systems, the physics of cuprates is between that of a doped AF Mott insulator (at weak doping) and that of a more conventional metal (described by the Fermi liquid theory in the overdoped regime). It is believed that their low energy properties could be described by a single band Hubbard model at intermediate coupling, so that electrons or holes can be either described as quasi-localized particles or waves. As a consequence, the spin excitations probed by INS measurements can be discussed using a spin localized picture or an itinerant one.

In the rest of the article, we are going to review a few inelastic neutron scattering results obtained in different families of superconducting cuprates. The purpose of the paper is definitively not to give an extensive review of all results which have been obtained so far. Excellent reviews can be found in Refs. [12,13]. We rather focus on the experimental observations which support the idea that there are residual magnetic interactions in the superconducting state of cuprates giving rise to unconventional spin triplet collective modes and that there is a strong *spin–fermion* coupling, which would be equivalent to the *electron–phonon* coupling in conventional superconductors (for a longer review see Ref. [14]). The paper is organized as follow. In Section 2, we report the observation of unconventional magnetic excitations in the superconducting state, using the inelastic neutron scattering technique: the so-called *resonant spin excitations*. In Section 3, we show that these unconventional excitations can be understood in the framework of spin band theory as a collective $S = 1$ mode existing in the superconducting state only: the *spin exciton*. In Section 4, we present anomalies in the charge excitation spectrum which are likely to involve the resonant spin excitations and thus can be viewed as the hallmark of the coupling of spin and charge degrees of freedom. In Section 5, we discuss the alternative interpretations of the resonant spin excitations using localized spin pictures.

2. Unconventional spin excitations in the superconducting state of cuprates

In the section, after a brief description of the inelastic neutron scattering technique, we show that this technique has been very useful in revealing the existence of unconventional magnetic collective modes in the superconducting state. Their characteristic energy is tightly related to the superconducting temperature or the superconducting gap as a function of hole doping. Furthermore, we show that the mode displays a very particular 'X'-like dispersion.

2.1. Inelastic neutron scattering technique

Since the AF properties of cuprates are likely to play a crucial role for the appearance of superconductivity in these materials, it turns out to be quite natural to try to study the evolution of the spin correlations as a function of hole doping, looking for experimental evidence that spin and charge properties are coupled. As pointed out in the previous section, the AF correlations are quickly destroyed upon hole doping, but dynamical short range AF correlations can still survive in the metallic or superconducting state. The inelastic neutron scattering technique is a powerful tool that allows us to study the spin correlations in a large range of momentum and energy. This is a bulk measurement that requires large single crystals. This constraint has for a long time restricted the study of the spin dynamics to a small number of cuprate families. Recently, thanks to progress made in crystal growth and the improvement of neutron flux, more and more cuprate families can be studied by inelastic neutron scattering, which is essential to establish the universality of the observed magnetic properties and thus their relevance for the physics of high temperature superconductors. Experiments can be carried out on high flux triple axis spectrometers (for instance at the ILL and LLB in France, at FRM-II in Germany) or on time-of-flight spectrometers (for instance, at ISIS in England).

The magnetic neutron scattering cross section per formula unit [15] is written in terms of the Fourier transform of the spin correlation function $S_{\alpha,\beta}(\mathbf{Q},\omega)$ (labels α, β correspond to Cartesian coordinates x, y, z) as:

$$\frac{\mathrm{d}^2\sigma}{\mathrm{d}\Omega\,\mathrm{d}\omega} = \frac{k_f}{k_i} r_0^2 F^2(Q) \sum_{\alpha,\beta} \left(\delta_{\alpha,\beta} - \frac{Q_\alpha Q_\beta}{|Q|^2}\right) S_{\alpha,\beta}(\mathbf{Q},\omega) \tag{3}$$

where k_i and k_f are incident and final neutron wave vectors, $r_0^2 = 0.292$ barns, $F(Q)$ is the magnetic form factor. The scattering vector $\mathbf{Q}$ can be split into $\mathbf{Q} = \mathbf{q} + \mathbf{G}$ where $\mathbf{q}$ lies in the first Brillouin zone and $\mathbf{G}$ is a wave vector of the Bravais lattice. Superconducting cuprates being nearly tetragonal systems, all reciprocal space coordinates (Q_x, Q_y, Q_z) (or (H, K, L)) are given in reduced lattice units $2\pi/a$, $2\pi/b$, $2\pi/c$, where $a \simeq b$ and c stand for the lattice parameters.

According to the fluctuation–dissipation theorem, the spin correlation function is related to the imaginary part of the dynamical magnetic susceptibility, weighted by the detailed balance factor:

$$S_{\alpha\beta}(\mathbf{Q},\omega) = \frac{1}{\pi(g\mu_B)^2} \frac{\mathrm{Im}\,\chi_{\alpha\beta}(\mathbf{Q},\omega)}{1-\exp(-\hbar\omega/k_BT)} \tag{4}$$

where g stands for the Landé factor. Note that in a paramagnetic state, when there is no spin anisotropy, $\mathrm{Im}\,\chi_{\alpha\beta}(\mathbf{Q},\omega)$ reduces to $\mathrm{Im}\,\chi(\mathbf{q},\omega)\delta_{\alpha\beta}$. $F(Q)$ is described by the anisotropic form factor of the Cu^{2+} ion in first approximation [16].

2.2. Magnetic resonance peak in the superconducting state

Using the INS technique to probe the spin dynamics in high temperature superconducting cuprates, one of the first major discoveries was the observation of an unusual magnetic excitation in the superconducting state: the so-called *magnetic resonance peak* [17–20]. The observation of this excitation was first reported by J. Rossat-Mignot et al. [17] in the superconducting system $YBa_2Cu_3O_{6.92}$ ($T_c = 91$ K). In the superconducting state, the magnetic resonance peak appears as a sharp excitation located at 41 meV (Fig. 3(a)) and is centered at the wave vectors $\mathbf{Q}_{AF} = (0.5, 0.5, L)$ (Fig. 3(b)), which characterized planar AF spin correlations. When increasing temperature, the characteristic energy of the magnetic resonance peak remains unchanged, whereas its intensity exhibits an order-parameter like temperature dependence and steeply disappears at T_c (Fig. 3(c)). Such a kind of excitation does not exist in conventional superconductors.

The observation of the magnetic resonance peak was then reproduced in other cuprate families. It is observed at optimal doping at 43 meV in $Bi_2Sr_2CaCu_2O_{8+\delta}$ ($T_c = 91$ K) [23] (Fig. 4(d)) and 47 meV in $Tl_2Ba_2CuO_4$ ($T_c = 90$ K) [21] (Fig. 4(a)). At least for superconducting cuprates, whose superconducting critical temperature can be as high as 90 K (Fig. 4), the existence of an unusual AF excitation in the superconducting state could be viewed as a generic property. While the magnetic resonance peak is almost resolution limited in $Tl_2Ba_2CuO_4$ and $YBa_2Cu_3O_{6.95}$ (Fig. 4(a), (b)), it is significantly broader in energy in $Bi_2Sr_2CaCu_2O_{8+\delta}$ (Fig. 4(b)). This energy broadening can be ascribed to intrinsic defects or impurities in the material and can be artificially reproduced by substitution of other $3d$ ions (such as Ni) in $YBa_2Cu_3O_7$ (Fig. 4(c)).

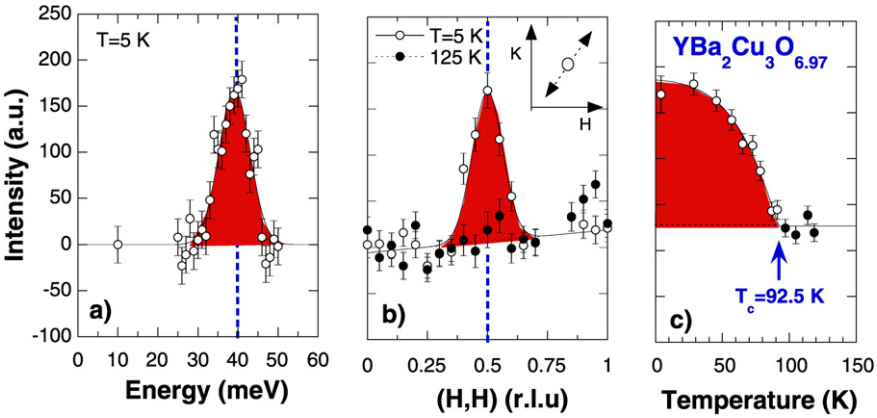

Fig. 3. Weakly overdoped $YBa_2Cu_3O_{6.97}$ ($T_c = 92.7$ K) [20]: (a) energy scan performed at the planar AF wave vector $\mathbf{Q}_{AF} = (0.5, 0.5)$ at 5 K in the superconducting state. (b) Constant energy scan at 40 meV performed along the (110) direction around $\mathbf{Q}_{AF}$ (see insert). At 5 K (open circles), a magnetic excitation, with a Gaussian line-shape, appears on top of a featureless nuclear background. At 125 K (solid dots), the magnetic signal disappears. (c) Temperature dependence of the magnetic intensity at 40 meV, that looks like the temperature dependence of an order parameter with a marked change at the superconducting critical temperature. This kind of temperature dependence is the hallmark of magnetic resonant excitations, which are intrinsic features of the superconducting state.

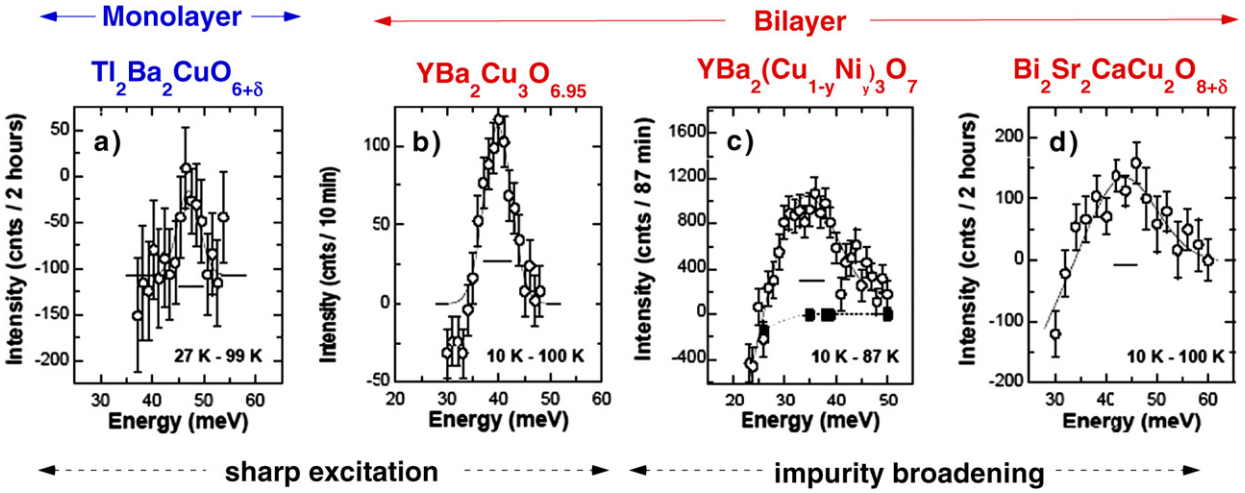

Fig. 4. The magnetic resonance is defined as the enhancement of the magnetic response in the superconducting state. Using unpolarized inelastic neutron scattering measurements, magnetic and nuclear scatterings are measured simultaneously. The magnetic resonance peak can, nevertheless, be extracted by performing the difference between measurements performed at low temperature in the superconducting state and just above T_c in the normal state. In the differential spectra, the magnetic resonance peak appears as a positive signal at a well defined energy, on top of a negative background, given by the thermal enhancement of the nuclear background. This procedure is particularly well suited when spin fluctuations of the normal state are weak compared to the resonance peak (optimal and overdoped regimes) (see Fig. 3(b)). The figure shows the difference spectrum of the neutron intensities at low temperature, measured at the planar AF wave vector $\mathbf{Q}_{AF} = (0.5, 0.5)$ and $T \geqslant T_c$ in samples: (a) $Tl_2Ba_2CuO_{6+\delta}$: $T_c \sim 90$ K, $V = 0.11$ cm^3 [21]; (b) $YBa_2Cu_3O_{6.95}$: $T_c = 93$ K, $V = 10$ cm^3 [19]; (c) $YBa_2(Cu_{1-y}Ni_y)_3O_7$: $T_c = 80$ K, $V \sim 2$ cm^3 [22]; (d) $Bi_2Sr_2CaCu_2O_{8+\delta}$: $T_c = 91$ K, $V = 0.06$ cm^3 [23]. V stands for the sample volume. Data are fitted to a Gaussian profile. The solid bars indicate the energy resolution.

2.3. *Several magnetic resonance peaks in multi-layer systems*

One may notice that the magnetic resonance peak is observed at slightly higher energy in $Tl_2Ba_2CuO_4$ which has only one CuO_2 per unit cell (monolayer system) (Fig. 4(a)), at variance with $YBa_2Cu_3O_{6+x}$ (Fig. 4(b)) or $Bi_2Sr_2CaCu_2O_{8+\delta}$ (Fig. 4(d)) which are characterized by two CuO_2 planes per unit cell (bilayer systems). This can be explained by the fact that there is not one but two resonant spin excitations in bilayer systems [24–27]. In slightly

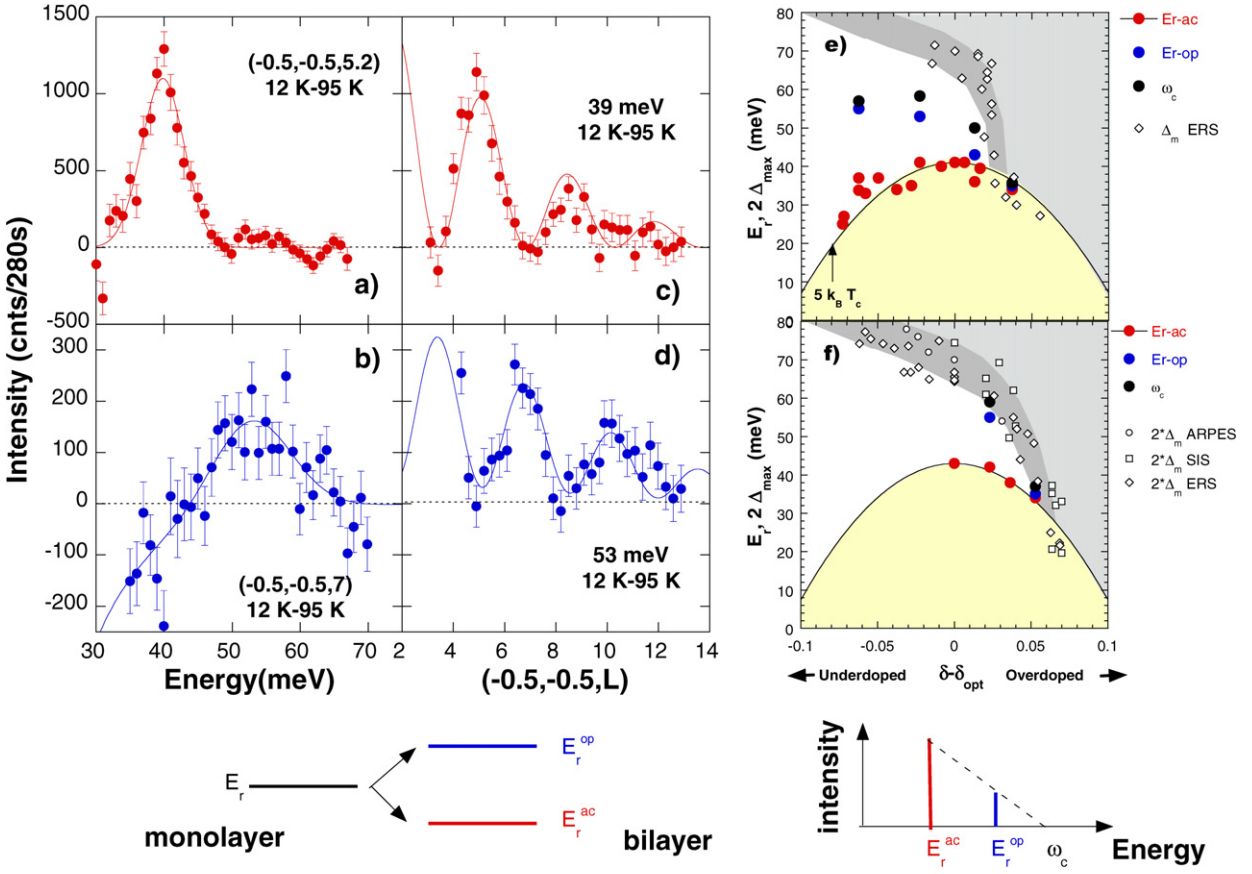

Fig. 5. In weakly underdoped $YBa_2Cu_3O_{6.85}$ ($T_c = 89$ K) [25], difference between scans measured at the AF wave vector at low temperature and just above T_c. (a), (c) The figures show the acoustic magnetic resonance peak (red) peaked at 41 meV and its typical sine square modulation. (b), (d) The optical magnetic resonance peak (blue), located at 53 meV and it characteristic cosine square modulation. The sketch below the figures (a)–(d) shows the splitting of the magnetic resonance peak induced by the magnetic interaction between the CuO_2 planes of the bilayer. (e), (f) Hole doping dependence of the characteristic energy of the acoustic (red) and optical (blue) magnetic resonance peaks [26,27]. Both modes are located below $2\Delta_m$ which gives the order of magnitude of the minimum energy required to create an elementary electron–hole spin flip excitation at the AF wave vector. $2\Delta_m$ (open symbols) can be measured by angle resolved photo-emission (ARPES), tunneling spectroscopy (SIS) or electronic Raman spectroscopy (ERS) (see Ref. [26,27] and references therein). Figure (e) shows the doping dependence in (Y,Ca)$Ba_2Cu_3O_{6+x}$ [26] and figure (f) in $Bi_2Sr_2CaCu_2O_{8+\delta}$ [27]. The hole doping level is obtained thanks to the phenomenological relationship: $T_c(\delta) = T_c^{\text{opt}}(1 - 82.6(\delta - \delta_{\text{opt}})^2)$ [4], δ_{opt} is generally estimated to be 0.16 [4]. The schematic picture below figures (e), (f) indicates how experimentally we extrapolate from the INS measurements of the resonance peaks the threshold of the electron–hole spin flip continuum, ω_c, which is expected to be slightly smaller that $2\Delta_m$. In (e), (f), black dots correspond to ω_c, deduced from INS data (see text).

underdoped $YBa_2CuO_{6.85}$ ($T_c = 89$ K) [25], the first magnetic resonance peak is observed at 41 meV (Fig. 5(a)) and a second one, of much weaker intensity, is found at 53 meV (Fig. 5(b)). The same observation has been recently reproduced in slightly overdoped $Bi_2Sr_2CaCu_2O_{8+\delta}$ ($T_c = 87$ K), where both excitations are observed at 42 meV and 54 meV, respectively [27]. One sees that both modes are located at ± 6 meV from 47 meV in $YBa_2Cu_3O_{6.85}$ and 48 meV in $Bi_2Sr_2CaCu_2O_{8+\delta}$, i.e. at equidistance from the energy at which the resonance spin excitation appears in the monolayer system with a similar superconducting critical temperature (insert in Fig. 5).

The existence of two resonance spin excitations in bilayer systems instead of one in monolayer systems is not very surprising. In the insulating parent compound, the spin excitations are collective: the spin waves. Owing to a weak AF interaction between CuO_2 planes in the bilayer ($J_\perp \simeq 10$ meV [12]), spin waves split into an acoustic mode and an optical one, corresponding to out-of-phase and in-phase spin fluctuations between the CuO_2 planes in the bilayer. The imaginary part of the dynamical spin susceptibility then reads:

$$\operatorname{Im}\chi(\mathbf{Q},\omega) = \sin^2(\pi z L)\operatorname{Im}\chi_{\text{ac}}(\mathbf{Q},\omega) + \cos^2(\pi z L)\operatorname{Im}\chi_{\text{op}}(\mathbf{Q},\omega) \tag{5}$$

where z stands for the reduced distance between CuO_2 planes in the bilayer ($z = d/c$ with $d = 3.3$ Å). In addition to the fact that acoustic and optical magnetic modes are located at different energies, they can be easily identified by the modulation of the magnetic intensity along the c axis (Eq. (5)). In the superconducting state, the stronger magnetic resonance peak at low energy displays a sine square modulation (Fig. 5(c)), whereas the weaker magnetic resonance peak at high energy exhibit a cosine square modulation (Fig. 5(d)). Thus, the existence of two resonance peaks in bilayer systems indicates that there is still an AF coupling between the CuO_2 planes in the superconducting state and that it has the same order of magnitude as $J_\perp$ in the insulating state. What is more surprising is the fact that the intensity of the optical-like excitation at high energy is significantly weaker than that of the acoustic-like excitation.

2.4. Hole doping dependence

One has to keep in mind that the superconducting state is a singlet spin state. In order to generate magnetic excitations, one needs to break Cooper pairs. In the d-wave superconducting state, the superconducting gap reads: $\Delta(k) = \Delta_m(\cos(k_x) - \cos(k_y))/2$, where Δ_m stands for the maximum of the superconducting gap. In superconducting cuprates, the minimum energy required to induce an elementary magnetic excitation at the AF wave vector is typically of the order of $2\Delta_m$. The latter energy can be measured by angle resolved photo-emission measurements (ARPES), tunneling scanning spectroscopy (SIS) or electronic Raman spectroscopy in B_{1G} channel (ERS) and is reported in Fig. 5(e), (f).

Let us consider now the hole doping dependence of the characteristic energy associated to acoustic and optical resonance peaks, E_r^{ac} and E_r^{op}, as compared to the hole doping dependencies of T_c and $2\Delta_m$ (Fig. 5(e), (f)). In bilayer systems, such as $YBa_2Cu_3O_{6+x}$ (Fig. 5(e)) and $Bi_2Sr_2CaCu_2O_{8+\delta}$ (Fig. 5(f)), E_r^{ac} is found to scale with the superconducting critical temperature T_c, so that $E_r^{\mathrm{ac}} \simeq 5k_BT_c$. At variance with the dome-like curve that characterizes the doping dependence of both E_r^{ac} and T_c, E_r^{op} levels off in the underdoped regime and further decreases when going from the optimal doping to the overdoped regime. The hole doping dependence of E_r^{op} displays striking similarities with the doping dependence of $2\Delta_m$. In the overdoped regime, for a doping level of $\sim$20%, E_r^{ac}, E_r^{op} and $2\Delta_m$ converge to the same energy, which is of the order of $5k_BT_c$ [26]. Below this doping level, one observes the following hierarchy: $E_r^{\mathrm{ac}} < E_r^{\mathrm{op}} < 2\Delta_m$. Therefore, it costs less energy to excite the resonance peak than to create elementary magnetic excitations by breaking Cooper pairs.

2.5. Unusual X-like lineshape of the resonant spin excitation dispersion

The magnetic resonance peaks are excitations which are observed in the superconducting state at the antiferromagnetic wave vector, but the observation of resonant spin excitations is not restricted to that particular wave vector [28–33]. On the other hand, it has been shown that the magnetic resonance peak is part of a dispersive $S = 1$ excitation mode [32] (Fig. 6(a)). Starting at the AF wave vector, the mode disperses downward and upward, yielding an X-like or hourglass-like dispersion [25,34,35]. One can also identify the so-called *silent bands* (blue dashed lines in Fig. 6(a)), which indicate that the intensity of dispersing $S = 1$ excitations disappears or is significantly reduced each time the mode approaches or crosses specific wave vectors [25]. In strongly underdoped cuprates ($T_c \leqslant 62$ K), similar dispersive excitations are also reported [36–40], but only the downward branch vanishes above T_c whereas the upward dispersion remains essentially the same across T_c [40]. Recently, the debate becomes focused on the origin of the $S = 1$ dispersive collective mode whose theoretical description is especially important as antiferromagnetism is generally believed to play a significant role in the superconducting pairing mechanism in high-T_c cuprates [8]. One possible way to account for the existence of a dispersive $S = 1$ collective mode in the d-wave superconducting state of superconducting cuprates is to describe the magnetic excitations as itinerant spin excitations.

3. Itinerant magnetic description of the resonant spin excitations: the spin exciton scenario

In this section, we give a description of the generalized magnetic susceptibility in the normal and the superconducting states using a spin itinerant model. We further show that, within this approach, the resonant spin excitations can be understood as a spin exciton. The comparison of neutron scattering experiments and the spin exciton model should allow us to quantitatively estimate the magnitude of the residual magnetic interaction left in the superconducting state.

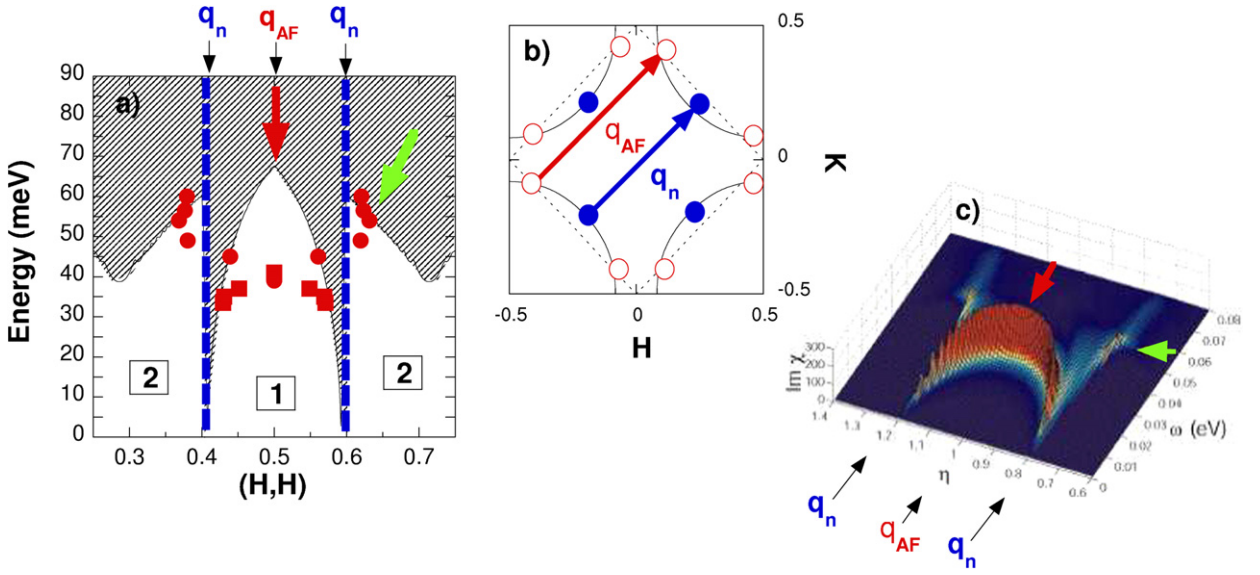

Fig. 6. (a) In weakly underdoped $YBa_2Cu_3O_{6.85}$ ($T_c = 89$ K), the acoustic resonant spin excitations disperse downward (squares [32]) and upward (circles [25]). The dashed region indicates the location of the *e–h* spin flip continuum, which is computed from ARPES measurements in $Bi_2Sr_2CaCu_2O_{8+\delta}$ for a similar doping level [51]. (b) Sketch of the Fermi surface. The red circles correspond to the *hot spots* at the Fermi surface, that can be connected by the AF wave vector $\mathbf{q}_{AF}$ and where the superconducting gap is almost maximum. The blue circles stand for the *cold spots* where the superconducting gap vanishes at the Fermi surface. Along the diagonal directions, the *cold spots* are connected by the wave vector $\mathbf{q}_n$. (c) Computation of the imaginary part of the dynamical magnetic susceptibility, Im χ, in the superconducting state within the spin exciton scenario [48]. The computed Im χ emphasizes the existence of a collective $S = 1$ mode located below the continuum, with two distinct branches (red and green arrows). The planar wave vector is written: $\mathbf{q} = \eta(0.5, 0.5)$. In (a) and (c), the red and green arrows indicate the parts of the dispersion which are located in area 1 and 2, which are defined in the text. The vertical dashed blue lines in (a) correspond to the so-called silent bands (see text and Refs. [25,48]).

3.1. Dynamical spin susceptibility in itinerant spin models

In a metal, one can create a magnetic excitation by transferring an electron from an occupied state $|k, \sigma\rangle$ to an unoccupied state $|k + q, -\sigma\rangle$. The non-interacting susceptibility, corresponding to these electron–hole (*e–h*) spin flip excitations, is given by the Lindhart function [15]:

$$\chi_0(\mathbf{q}, \omega) = \frac{1}{2}(g\mu_B)^2 \sum_k \frac{n^F(\bar{\xi}_k) - n^F(\bar{\xi}_{k+q})}{\bar{\xi}_{k+q} - \bar{\xi}_k - \hbar\omega - i0^+} \tag{6}$$

$\bar{\xi}_k$ is defined as a function of ξ_k the bare quasi-particle dispersion and the chemical potential μ: $\bar{\xi}_k = \xi_k - \mu$. n^F corresponds to the Fermi distribution. χ_0 stands for $\chi^{xx} = \chi^{yy} = \chi^{zz}$. In the superconducting state (with spin singlet Cooper pairs), the non-interacting spin susceptibility transforms into the BCS function [14]:

$$\chi_0^{\mathrm{BCS}}(\mathbf{q}, \omega) = \frac{1}{2}(g\mu_B)^2 \sum_k M_{qk}^{\mp} \frac{1 - n^F(E_{k+q}) - n^F(\pm E_k)}{E_{k+q} \pm E_k - \hbar\omega - i0^+} \tag{7}$$

with:

$$M_{qk}^{\pm} = \frac{1}{4}\left(1 \pm \frac{\bar{\xi}_{k+q}\bar{\xi}_k + \Delta_{k+q}\Delta_k}{E_{k+q}E_k}\right) \tag{8}$$

where $E_k = \sqrt{\bar{\xi}_k^2 + \Delta_k^2}$ is the dispersion relation of the quasi-particles in the superconducting state and Δ_k the momentum dependent superconducting gap. It is worth noticing that Eq. (7) becomes Eq. (6) when $\Delta_k \to 0$. There are two main differences between the Lindhart and the BCS spin susceptibility. First, a minimum energy $\hbar\omega_c(q) = \min[E_{k+q} + E_k]$ is needed to create an elementary spin flip excitation in the superconducting state. $\hbar\omega_c(q)$ defines the threshold of the electron–hole spin flip continuum. Second, spin excitations are two-particles processes

and the coherence factor (Eq. (8)) in the superconducting state is an *interference*-term that probes the sign change of the superconducting order parameter: $\Delta_{k+q}\Delta_k < 0$ favors spin excitations. For a d-wave superconducting gap $\Delta_k = \Delta_m(\cos(k_x) - \cos(k_y))/2$, this condition is fulfilled around the planar AF wave vector $(0.5, 0.5)$ $(= (\pi, \pi))$.

The magnetic response is further enhanced by magnetic interaction $I(q)$. This interaction is, for instance, U the on-site Coulomb repulsion in single band Hubbard model or $-J(q)$ in the t–J model (see Section 1). The enhanced spin susceptibility can be obtained by random phase approximation (RPA):

$$\chi(\mathbf{q},\omega) = \frac{\chi_0(\mathbf{q},\omega)}{1 - \frac{2I(q)}{(g\mu_B)^2}\chi_0(\mathbf{q},\omega)} \tag{9}$$

In the absence of specific topological properties of the Fermi surface (such as nesting or vicinity of a saddle point) or of very strong interaction $I(q)$, the magnitude of the spin excitation spectrum can remain rather weak and is therefore difficult to probe by INS measurements. In the superconducting state [41–48], owing to the opening of a gap in the e–h spin flip continuum and magnetic interaction $I(q)$, an e–h spin triplet bound state, also called spin exciton, can develop below the threshold of the continuum. Its characteristic energy is given by the pole condition: $1 - \frac{2I(q)}{(g\mu_B)^2} Re\,\chi_0(\mathbf{q},\omega) = 0$ in the energy range $[0, \omega_c(\mathbf{q})]$.

3.2. Dispersion of the spin exciton: the fingerprint of the gapped Stoner continuum

This $S = 1$ collective mode can only exist below the e–h spin flip continuum and decays into elementary e–h excitations when entering the continuum. The dispersion of the mode is therefore mainly controlled by the momentum dependencies of the magnetic interaction $I(q)$ and the threshold of the continuum $\omega_c(\mathbf{q})$. The latter is given by the topology of the Fermi surface and the symmetry of the superconducting gap. In superconducting cuprates, $\omega_c(\mathbf{q})$ is maximum at the AF wave vector: $\omega_c(\mathbf{q}_{AF}) = 2\Delta(\mathbf{k}_{hs})$, where $\mathbf{k}_{hs}$ are the wave vectors of the Fermi surface that can be connected by the AF wave vector $\mathbf{q}_{AF}$, also called *hot spots* (*hs*) (Fig. 6(b)). At these wave vectors, the d-wave superconducting gap is large and close to its maximum value, so that $\omega_c(\mathbf{q}_{AF})$ is slightly smaller than $2\Delta_m$. Moving away from the AF wave vector in the [110] direction (Fig. 6(c)), $\omega_c(\mathbf{q})$ decreases and vanishes at $\mathbf{q}_n$ the wave vector between the nodal points of the Fermi surface (the *cold spots*) (Fig. 6(b)), where the superconducting gap goes to zero. Thus, around the AF wave vector, $\omega_c(\mathbf{q})$ displays a dome-like line-shape (area 1) (Fig. 6(a)). Away from the wave vector $\mathbf{q}_n$, $\omega_c(\mathbf{q})$ re-appears at high energy (area 2) (Fig. 6(a)). In area 1, the collective mode cannot disperse upwards and is pushed to a low energy by the continuum and finally exhibits a characteristic downward dispersion (red arrow in Fig. 6(a), (c)). When moving from area 1 to area 2, $\omega_c(\mathbf{q})$ goes steeply to zero close to $\mathbf{q}_n$. As a consequence, the spin exciton has to vanish when approaching some almost energy independent lines centered at $\mathbf{q}_n$: the so-called *silent bands* (dashed lines in Fig. 6(a)). In area 2, a second part of the collective mode of much weaker intensity shows up at higher energy with a upward dispersion (green arrow in Fig. 6(a), (c)). It has been shown that the spin exciton in area 1 can be viewed as a linear combination of direct e–h spin excitations, whereas in area 2 it is made of umklapp spin excitations [48].

The fact that the magnetic resonance peak observed by INS measurements is an intrinsic feature of the superconducting state can be understood within the spin exciton scenario. Likewise, the confinement of the spin exciton below the threshold of the e–h spin flip continuum (Fig. 6(a), (c)) provides an explanation for the downward and upward dispersion of the magnetic resonant excitations. The observation of *silent bands* in INS data [25] can be viewed as the fingerprint of the continuum close to $\mathbf{q}_n$ (Fig. 6(a)).

3.3. What can we learn from the observation of two resonance peaks in bilayer systems?

In addition to the dispersion of the magnetic resonant mode, the intensity of the resonant excitations observed in INS measurements supports the spin exciton scenario. The imaginary part of the dynamical spin susceptibility close to $\Omega_r(\mathbf{q})$ the energy of the triplet bound state reads:

$$\mathrm{Im}\,\chi(\mathbf{q},\omega>0) = \pi \frac{1}{(\frac{2I(q)}{g\mu_B})^2}\left(\frac{d\,Re\,\chi_0(\mathbf{q},\omega)}{d\omega}\bigg|_{\omega\to-\Omega_r(\mathbf{q})}\right)^{-1}\delta\big(\omega - \Omega_r(\mathbf{q})\big) \tag{10}$$

At $\omega_c(\mathbf{q})$, $\mathrm{Im}\,\chi_0(\mathbf{q},\omega)$ is a step-function and $Re\,\chi_0(\mathbf{q},\omega)$, which is given by Kramers–Kronig relationship, displays a logarithmic divergence at the threshold of the e–h continuum: $Re\,\chi_0(\mathbf{q},\omega) \simeq Re\,\chi_0(\mathbf{q},0) - \beta\ln(|\frac{\omega_c(\mathbf{q})-\omega}{\omega_c(\mathbf{q})}|) + \cdots$. As

a consequence, the spectral weight of the triplet bound state appears to be proportional to the reduced binding energy $(\omega_c(\mathbf{q}) - \omega)/\omega_c(\mathbf{q})$ [52]:

$$\operatorname{Im}\chi(\mathbf{q}, \omega > 0) \simeq \pi \frac{1}{(\frac{2I(q)}{g\mu_B})^2} \frac{1}{\beta} \frac{\omega_c(\mathbf{q}) - \omega}{\omega_c(\mathbf{q})} \delta\big(\omega - \Omega_r(\mathbf{q})\big) \tag{11}$$

Thus, the closer the mode is to the continuum, the weaker its intensity is. In the case of bilayer systems, this property explains why the intensity of the acoustic resonance peak at low energy is always stronger than that of the optical resonance peak (second schematic picture below in Fig. 5(e), (f)). Furthermore, one can get the advantage of the existence of two resonance peaks in bilayer systems. For these systems, $I(q) = I_{\parallel}(q) \pm I_{\perp}$, where $I_{\parallel}(q)$ is the planar magnetic interaction and $I_{\perp}$ a weak inter-plane magnetic interaction. At the AF wave vector $I_{\parallel}(q_{AF}) \gg I_{\perp}$, one can therefore neglect $I_{\perp}$ in a first approximation. As a second approximation, one can assume that the electronic bands in each of the CuO_2 planes of the bilayer are degenerated, so that the threshold of the continuum is the same for each band. Under these assumptions, one finds according to Eq. (11) that the ratio of the energy integrated spectral weight of the acoustic and optical modes, $R = W_r^{ac}/W_r^{op}$ is equal to $(\omega_c(\mathbf{q}_{AF}) - E_r^{ac})/(\omega_c(\mathbf{q}_{AF}) - E_r^{op})$. At the AF wave vector, the threshold of the continuum can thus be directly estimated from INS measurements [24–27]:

$$\omega_c(\mathbf{q}_{AF}) = \frac{E_r^{op} R - E_r^{ac}}{R - 1} \tag{12}$$

When R is large, $\omega_c(\mathbf{q}_{AF})$ and E_r^{op} are close to each other. In addition, $\omega_c(\mathbf{q}_{AF})$ should be slightly smaller than $2\Delta_m$ as found experimentally. This is the reason why both $\omega_c(\mathbf{q}_{AF})$ and E_r^{op} display a hole doping dependence very similar to that of $2\Delta_m$ (Fig. 5(e), (f)). In $YBa_2Cu_3O_{6+x}$, where ARPES measurements that probe the electronic spectrum are still in progress [2,49], comparisons between theory and INS experiments therefore remain qualitative. Nevertheless, for four doping levels, $\omega_c(\mathbf{q}_{AF})$, E_r^{op} and E_r^{ac} were determined and after calibration of the magnetic intensity in absolute units, it was found that the energy integrated spectral weight of the resonance peaks scale with the reduced binding energy, with a scaling factor which is hole doping independent within experimental accuracy [26]. In $Bi_2Sr_2CaCu_2O_{8+\delta}$, ARPES data are available (see Ref. [14]) and the recent estimates of $\omega_c(\mathbf{q}_{AF})$ from INS data at optimal doping and in the overdoped [27,50] regime match quite well the values that can be computed from ARPES measurements [51].

The overall doping dependence of E_r^{ac} and E_r^{op} can be well reproduced within the exciton scenario [54,55]. From these studies, one can get a phenomenological description of the magnetic interaction $I(q)$: $I_{\parallel}(q) = I_0(1 - 0.1(\cos(k_x) + \cos(k_y))$ and $I_{\perp} = 0.027 I_0$. The typical order of magnitude of I_0 is about 560 meV, assuming that the nearest neighbor hopping parameter t is ~ 250 meV as measured by ARPES and therefore significantly renormalized as compared to the LDA calculations ($t = 400$ meV). In the t–J model, one would expect $I(q)$ to be $-J(q)$ the planar AF superexchange interaction found in the insulating AF state: $J(q) = 2J(\cos(k_x) + \cos(k_y))$ ($J \simeq 100$–140 meV). At the AF wave vector, $J(\mathbf{q}_{AF}) = -4J$ is of the same order magnitude as I_0 and the rations $J_{\perp}/4J$ and $I_{\perp}/I_0$ are similar. On the other hand, it seems that the momentum dependence of the interaction in the superconducting state is much less marked. The interaction is even almost q-independent, as the on-site Coulomb repulsion U in the Hubbard model. Thus, using the spin exciton scenario in the same way as one usually uses spin wave model to describe collective spin excitations in an ordered magnet, one can extract from INS data the characteristic strength and momentum dependence of the magnetic interaction left in the superconducting state. This should help to select the Hamiltonian that must be used to describe the magnetic and electronic properties.

4. Anomalies in the charge excitation spectrum: the feedback effect

For the traditional low-temperature superconductors, anomalies in tunneling I–V characteristics as well as in the optical conductivity $\sigma_1(\omega)$, when combined with neutron scattering data on the phonon density of states, provided detailed evidence that the pairing in these materials was mediated by the exchange of phonons [56]. In this section, we show that several anomalies observed in tunneling spectroscopy, angle resolved photoemission measurements and optical conductivity can be associated with the resonant spin excitation, indicating the existence of a *spin–fermion* coupling in cuprates, which could play the same role as the *electron–phonon* coupling in traditional low-temperature superconductors.

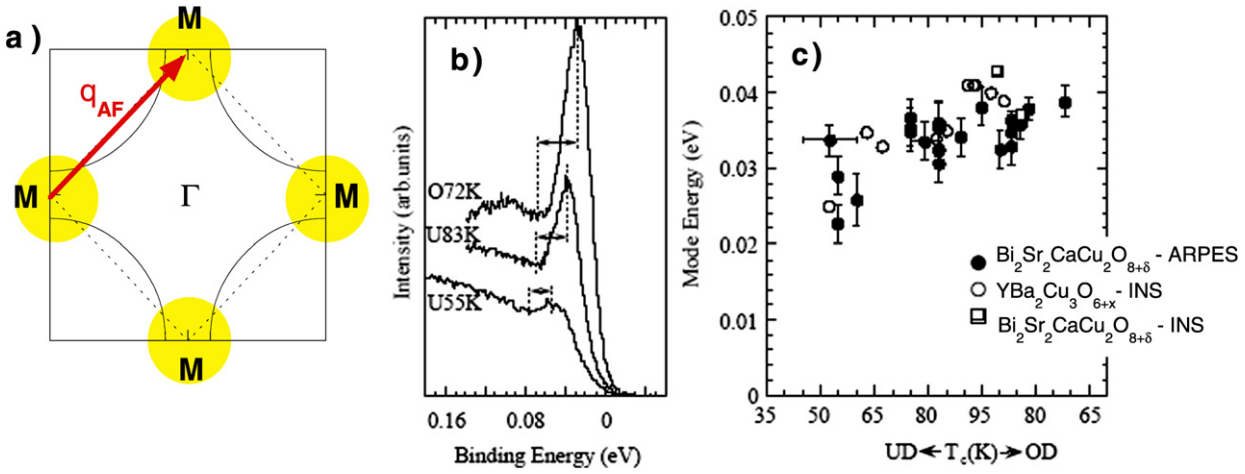

Fig. 7. (a) Sketch of the Fermi surface. (b) ARPES spectra in $Bi_2Sr_2CaCu_2O_{8+\delta}$ at the M point for different doping levels. ARPES data correspond to measurements carried out in two underdoped samples (U) with $T_c = 55$ K and 83 K and one overdoped sample (O) with $T_c = 72$ K. The dashed lines indicate the separation between the peak and the dip [57]. (c) The collective mode energy as deduced from ARPES data and the energy of the magnetic resonance peak as a function of the superconducting critical temperature from the underdoped (UD) to the overdoped (OD) regimes [57].

For cuprates, several anomalous features have been reported in the charge excitation spectrum, in particular by ARPES and tunneling measurements (for a review, see Ref. [14]). In ARPES data, the charge excitation spectrum close to the *hot spots* exhibits an anomalous peak-dip-hump structure (Fig. 7(b)), with the peak located at the energy of E_k which is close to Δ_m for these states. Since the anomaly disappears in the normal state, it is ascribed to the scattering of quasi-particles by a collective mode of energy Ω, which may exist in the superconducting state only. The anomaly in charge excitation spectrum should start at an energy $\sim\Delta_m + \Omega$, i.e. the energy needed to create a quasi-particle out of the superconducting condensate plus the energy of the collective mode. It is at this energy that the dip should appear. Experimentally, the energy difference between the peak and the dip is found at the same energy as the acoustic magnetic resonance peak and further displays the same hole doping dependence, i.e. it scales with $\sim 5k_B T_c$ (Fig. 7(b)) [57]. In addition, the anomaly is observed close to the *hot spots*, which are connected by the AF wave vector and where there is a large density of states, due to the vicinity of a van Hove singularity (Fig. 7(a)). A similar peak-dip-hump structure is observed in the tunneling spectra [58] and, once again, the energy difference between the peak and the dip matches the energy and the doping dependence of the acoustic resonance peak. The optical conductivity measurements also provide evidences of a coupling of the resonant spin excitations with charge carriers [59].

Thanks to the improvement of ARPES measurements [14,60], it is now possible to observe the splitting of the electronic bands into bonding (B) and anti-bonding bands (A) in $Bi_2Sr_2CaCu_2O_{8+\delta}$. This splitting is the consequence of a finite hopping of quasi-particles between the CuO_2 planes in the bilayer, which lifts the degeneracy of the bands. The peak-dip-hump anomaly is mainly observed in the B band. Close to the *hot spots*, the density of states is higher in the A band than in the B band, thus in order to obtain a stronger anomaly in the B band the mode involved in the scattering process must couple the A and B bands. It turns out that the acoustic resonance mode, which has the stronger spectral weight, corresponds to inter-band e–h spin excitations (AB, BA), whereas the optical mode requires intra-band e–h spin excitations (BB, AA) [53–55]. This property explains why the peak-dip-hump feature is mainly observed in the B band, as the result of the scattering of the quasi-particles of the A band by the strong acoustic spin resonant mode [14,60].

In addition, it is known that substitution of Cu by other transition metals, such as Zn or Ni, reduces T_c [61,62]. In Zn or Ni substituted $YBa_2Cu_3O_{6+x}$, INS measurements show that the acoustic resonance peak broadens and its intensity weakens, with a minor change of its characteristic energy [22,63–65]. Recent ARPES measurements [66], performed in Ni or Zn substituted $Bi_2Sr_2CaCu_2O_{8+\delta}$, indicate that the dip feature is smeared out, as expected for the damping of the mode involved in the scattering of quasi-particles.

There is now a consensus that the anomalies in the charge excitation spectrum are due to the coupling to a collective mode [10,14,67], but the origin of the collective mode is still matter of discussion. Is it a phonon or the magnetic

resonance peak? Its temperature dependence, its characteristic energy, its symmetry and its sensitivity to Ni and Zn impurities suggest that the magnetic resonance peak must be this mode. The observation of anomalies in the charge excitation spectrum due to the magnetic resonance peak is a feedback effect. The magnetic resonance peak is a quasi-particle–hole bound state, that appears as a consequence of the opening of the superconducting gap and residual AF interaction. As soon as the mode settles in, it interacts with the quasi-particles in the superconducting state. This feedback effect highlights the existence of a *spin–fermion* coupling in high temperature superconducting cuprates, that couples spin and charge degrees of freedom, as the *electron–phonon* coupling couples lattice and charge degrees of freedom in conventional superconductors. Thus, the observation of resonant spin excitations in the superconducting state by INS measurements shows (i) that there are residual magnetic interactions left in the superconducting state, otherwise the resonant spin collective mode would not exist, and (ii) that a rather strong *spin–fermion* coupling exists, whose magnitude should of the order of $\sim$1 eV [14,67].

However, one should not conclude that the resonant spin excitations play the role of the glue of the Cooper pairs in the superconducting state. Indeed, the magnetic resonance peak exists only in the superconducting state, and it is believed that the fluctuations involved in the pairing mechanism should pre-exist in the normal state, as the phonons in conventional superconductors. In the spin fluctuation exchange pairing mechanism, the fluctuations of the continuum should trigger superconductivity thanks to *spin–fermion* coupling. In the t–J model, the same exchange interaction $J(q)$, which should be responsible for the appearance of the resonant spin mode, should play also the role of a direct attractive interaction (eventually further enhanced by AF fluctuations). Whatever the exact mechanism that triggers superconductivity, once superconductivity develops, resonant spin excitations modify the charge spectrum and thus strongly influence the superconducting state.

5. Origin of the $S = 1$ collective mode: beyond the itinerant picture

Using a spin band model, we have seen that one can account for the existence of resonant spin excitations. This approach seems to be well suited for the overdoped regime and close to optimal doping. However, it is running into trouble in the well underdoped regime or for the description of the magnetic properties of $La_{2-x}Sr_xCuO_4$ system. In this section, we give some routes to go beyond this approach.

5.1. From itinerant spin picture to localized spin picture

Starting from the metallic side of the phase diagram of high-T_c superconductors and reducing the hole doping, one can understand the $S = 1$ collective mode within an itinerant-spin model. The resonant magnetic collective mode can be described as *a spin exciton* [14,41–48], i.e. a $S = 1$ bound state, pushed by AF interaction below the gaped e–h spin flip continuum in superconducting state. Alternatively, when starting from the Mott-insulator side of the phase diagram and increasing the hole doping, the mode can be viewed as reminiscent of magnons observed in the insulating AF state: this corresponds to the localized-spin models [68,69]. The collective modes between localized spins on Cu sites that may survive are heavily damped by the scattering by charge carriers. Long-lifetime collective excitations can be restored in the superconducting state, when scattering processes are eliminated below the gaped e–h spin flip continuum. On the contrary, when the collective mode between localized spins remains inside the continuum in the superconducting state, the low energy excitations become of excitonic type: the itinerant-spin approach is recovered [68,69]. Both approaches may represent two different limits of a more global description that considers the magnetism of high-T_c superconductors of dual character: both localized spins and itinerant spins are actually tightly bound and cannot be disentangled [70,71]. It is worth emphasizing that in a dual approach one can schematically ascribe the upper dispersion to the localized character of the magnetic response and the lower one to the itinerant one. In all these models, the change of the band electronic excitations passing through T_c has an important feedback on the spin excitation spectrum in the superconducting state.

The magnetic resonance peak exists in hole doped cuprates whose maximum T_c is about 90 K. More recently, the magnetic resonance peak has also been observed in an electron doped system $Pr_{0.88}LaCe_{0.12}CuO_4$ at 12 meV ($T_c = 24$ K) [72]. There is still a debate concerning its existence in the hole doped mono-layer system $La_{2-x}Sr_xCuO_4$ with a maximum of T_c of $\sim$ 37 K. The magnetic excitations in that compound are rather strong even in the normal state and located at incommensurate planar wave vectors $(0.5(1 \pm \delta_{inc}), 0.5)$ and $(0.5, 0.5(1 \pm \delta_{inc}))$ [13,73]. This is in marked contrast with both the hole-doped and electron doped systems mentioned above, for which the normal

state magnetic fluctuations (if observable) remain centered around the planar AF wave vector (0.5, 0.5) [40,75,76,72]. However, passing through T_c, the incommensurate spin fluctuations of $La_{2-x}Sr_xCuO_4$ are enhanced and become narrower in momentum space, in an energy range which is about $5k_BT_c$ [74]. This phenomenon, usually referred to as a *coherence effect*, and the resonance peak could eventually share a common origin and could be viewed as excitonic $S = 1$ modes, with different dispersions. However, the spin excitation spectrum in $La_{2-x}Sr_xCuO_4$ usually is not described using an itinerant spin picture, but rather using a localized one, which involves spatial inhomogeneous distribution of localized spin on copper and doped holes: the so-called stripe model [13,77].

5.2. *Heterogeneous charge distribution: the stripe picture*

The stripe model (see Ref. [77] and references therein) considers that in a $S = 1/2$ AF Heisenberg system, doped holes segregate to form lines of charge, separating hole-poor AF domains in anti-phase. The metallic state is viewed as a disordered stripe phase, where charged lines can fluctuate (Fig. 8(a), (b)). It is worth noticing that in the stripe model, charge excitations are collective modes, so that spin excitations made of fermionic excitations (i.e. e–h spin flip excitations) do not exist. The physical interpretation of the spin–spin correlations is at the opposite of the spin band picture discussed in the previous sections.

Static stripes can be easily identified in X-ray and neutron diffraction measurements. They indeed give rise to superstructure charge peaks at $(0, \pm 2\delta_{inc})$ (or $(0, \pm 2\delta_{inc})$) and superstructure magnetic peaks at vectors $(0.5(1 \pm \delta_{inc}), 0.5)$ (or $(0.5, 0.5(1 \pm \delta_{inc}))$). Diffraction patterns consistent with static stripes are observed in $La_{15/8}Ba_{1/8}CuO_4$ [78] and $(La,Nd)_{2-x}Sr_xCuO_4$ [79]. In these systems, a structural transition (the so-called LTT phase) has been proposed to pin static stripes. In $La_{2-x}Sr_xCuO_4$, stripes may remain fluctuating, not being pinned by the lattice (LTO phase).

Based on the spin dynamics data in the stripe ordered system $La_{15/8}Ba_{1/8}CuO_4$ (Fig. 8(c)), it has been proposed that, at the AF wave vector, E_r could be a saddle point in the dispersion with spin excitations propagating along a given direction (say a^*) below E_r and along the direction perpendicular (i.e. b^*) above E_r [13,80], giving rise to

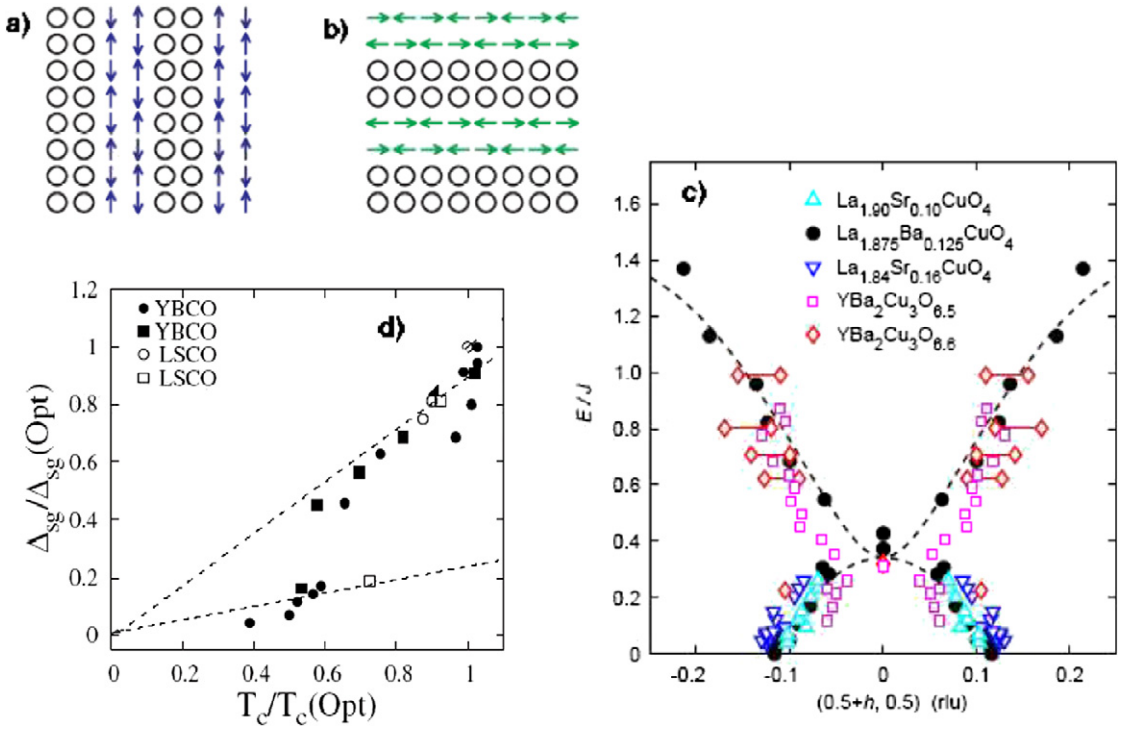

Fig. 8. (a), (b) Bond-centered stripe model according to which non-magnetic charge stripes separate a set of weakly coupled 2-leg spin ladders in the copper oxide layers. (c) Comparison of the dispersions of spin excitations in non-superconducting $La_{15/8}Ba_{1/8}CuO_4$, in superconducting $La_{2-x}Sr_xCuO_4$ and $YBa_2Cu_3O_{6+x}$. Figures (a)–(c) are reproduced from Ref. [13]. (d) Spin gap, Δ_{sg} in superconducting $La_{2-x}Sr_xCuO_4$ (LSCO: open symbols) and $YBa_2Cu_3O_{6+x}$ (YBCO: full symbols) (see [86] and references therein). The upper dashed line correspond to $\Delta_{sg} \simeq 3.8k_BT_c$.

an X-like line-shape in twinned crystals where a^* and b^* are mixed. More precisely, this system is characterized by a spin and charge stripe order at low temperature: the spin excitations spectrum can then be modeled by a specific bond-centered stripe model according to which non-magnetic charge stripes separate a set of weakly coupled 2-leg spin ladders in the copper oxide layers (Fig. 8(a), (b)). The low energy excitations (below E_r) correspond to collective excitations between coupled spin ladders, running across the stripe directions, whereas the high energy part of the spectrum (above E_r) is associated with intra-spin ladder excitations propagating parallel to the lines of charges. This picture, sustained later by calculations [81–84], implied a pronounced in-plane anisotropy of the magnetic spectrum.

The spin excitation spectra as measured in $La_{15/8}Ba_{1/8}CuO_4$, in $La_{2-x}Sr_xCuO_4$ and in $YBa_2Cu_3O_{6+x}$ display a striking similarity, as shown in Fig. 8(c). It has been therefore proposed that spin excitation spectra in cuprates could be universal and that the X-like lineshape is the hallmark of static or dynamical stripes [13,85]. To account for the absence of an enhancement of the magnetic response at E_r in $La_{2-x}Sr_xCuO_4$ in contrast to the other systems, the following phenomenological scenario has been suggested, [13]. In the superconducting state, low energy spin fluctuations are suppressed below a characteristic energy, the *spin-gap* $\Delta_{sg} \simeq 3.8k_BT_c$. When the spin gap opens, there should be a transfer of spectral weight from energies below Δ_{sg} to energies above Δ_{sg}. When Δ_{sg} is slightly below E_r, the magnetic response is enhanced at E_r in the superconducting state: this could be the case for $YBa_2Cu_3O_{6+x}$. On the other hand, when Δ_{sg} is at much lower energy than E_r, the enhancement of the magnetic susceptibility does not take place at E_r: this should be the case of $La_{2-x}Sr_xCuO_4$.

As pointed out, the spin excitation spectrum should display a strong 1D anisotropy, which should be hidden in twinned samples. This is in contrast to the leading symmetry of the spin excitations in underdoped and optimally doped $YBa_2Cu_3O_{6+x}$ [39,40]. Indeed, using detwinned $YBa_2Cu_3O_{6+x}$ samples [40], it has been proved that the spin excitations spectrum exhibits a 2D symmetry both below [39] and above [40] E_r, inconsistent with a saddle-point dispersion. Furthermore, if the X-like dispersion exits even in non-SC state, as in $La_{15/8}Ba_{1/8}CuO_4$, it is more meaningful to compare the spectrum in non-SC $La_{15/8}Ba_{1/8}CuO_4$ with the magnetic spectrum of the normal state in SC cuprates as it has been recently done in underdoped $YBa_2Cu_3O_{6.6}$ [40]. The conclusion of this study is that the normal state spin fluctuations do not display the same dispersion as in $La_{15/8}Ba_{1/8}CuO_4$. The dispersion evolves from a X-like to a Y-like lineshape when passing through T_c. This study does not rule out dynamical stripes. However, it points out that it is not easy to define which part of the spin excitation spectrum is really common to all cuprates. Actually, in underdoped cuprates, only the high energy part of spectrum (upper dispersion) seems to be universal and seems somehow reminiscent of the spinwaves of the AF insulating state (remaining localized spin response).

In addition, it is worth noticing that the computation of the spin dynamics in the framework of the stripe model was first performed for a monolayer system [81–84] and later extended to the case of a bilayer system [87,88]. These computations indicate that charge lines should not lie on top of each other in a bilayer, in order to minimize their Coulomb repulsion. As a consequence, the acoustic and optical spin excitations cannot be described anymore by Eq. (5), in contrast with INS data in bilayer systems. The observed momentum dependence of the acoustic and optical spin excitations in bilayer systems questions the theoretical predictions based on a stripe model.

Thus, it is not yet clear whether the $La_{2-x}(Sr,Ba)_xCuO_4$ system should be viewed as a proto-type system for cuprates, revealing the central role of stripes, or as a peculiar system where the coupling of spin and charge degrees of freedoms with the lattice favors spin- and charge-density waves.

6. Concluding remarks

In conventional superconductors, the neutron scattering technique has been used to study the vortex lattice in the superconducting state, the phonon density and the renormalization of phonons in the superconducting state. Similar studies are also performed in high temperature superconductors, but the possibility of a superconducting pairing mediated by magnetic properties has stimulated an unprecedented study of the spin excitation spectrum in these systems by using neutron scattering.

We have shown how, in the superconducting state, the inelastic neutron scattering technique has brought to light the existence of an unusual $S = 1$ spin collective mode. Using an itinerant approach, this excitation can be understood as a spin exciton. This excitation may further interact with quasi-particles in the superconducting state, yielding anomalies in the charge excitation spectrum, that are observed by angle resolved photo-emission and tunneling spectroscopy. If an itinerant approach can account for the main features of the spin excitation spectrum close to optimal doping, its relevance becomes more questionable in the strongly underdoped regime or for systems where T_c is reduced: localized

spin degrees of freedom should be considered. A unique theoretical model that can capture all peculiarities of the spin excitation spectra measured by INS in different cuprate families is still required in order to conclude about the role of spin fluctuations in the appearance of *d*-wave superconductivity [10].

Finally, we mainly focused on the spin excitations in the superconducting state and ignored the normal state properties. Indeed, if the understanding of unconventional superconductivity remains a major challenge for condensed matter physicists, the description of the normal state properties is as challenging since they are not *normal* at all. Cuprates behave as conventional metals only in the overdoped regime (Fermi liquid state). Close to optimal doping they display exotic electronic properties, such as a resistivity linear as a function of temperature at any temperature (non-Fermi liquid state). In the underdoped regime, below a certain temperature T^*, the systems enter a state characterized by the opening of a pseudo-gap in both spin and charge excitation spectra (pseudo-gap state) (Fig. 1). The origin of these anomalous electronic properties in the normal state is subject to intense theoretical and experimental studies [89–91], but no consensus has yet been achieved. Interestingly, whatever the theoretical proposal for the pseudo-gap state, there is always a magnetic signature that should be checked by elastic or inelastic neutron scattering. Among various theoretical proposals, it has been proposed in particular that the pseudo-gap state is a new state of matter, implying the existence of circulating nanoscopic currents and these circulating currents can be detected by elastic neutron scattering (for a review, see Ref. [92]).

References

[1] M. Imada, A. Fujimori, Y. Tokura, Rev. Mod. Phys. 70 (1998) 1039–1263.
[2] A. Damascelli, Z. Hussain, Z.X. Shen, Rev. Mod. Phys. 75 (2003) 473.
[3] P.A. Lee, N. Nagaosa, X.G. Wen, Rev. Mod. Phys. 78 (2006) 17.
[4] J.L. Tallon, C. Bernhard, H. Shaked, R.L. Hitterman, J.D. Jorgensen, Phys. Rev. B 51 (1995) 12911–12914.
[5] D.J. Van Harlingen, Rev. Mod. Phys. 67 (1995) 515–535.
[6] F.C. Zhang, C. Gros, T.M. Rice, H. Shiba, Supercond. Sci. Technol. 1 (1988) 36–46.
[7] G. Kotliar, J. Liu, Phys. Rev. B 38 (1988) 5142.
[8] See e.g., D. Scalapino, Phys. Rep. 250 (1995) 329.
[9] A.-M.S. Tremblay, B. Kyung, D. Sénéchal, Low Temp. Phys. 32 (2006) 424.
[10] M.R. Norman, Contribution to the Handbook of Magnetism and Advanced Magnetic Materials, vol. 5, Wiley, cond-mat/0611422.
[11] P.E. Sulewsky, P. Fleury, K. Lyons, S. Cheong, Z. Fisk, Phys. Rev. B 41 225.
[12] P. Bourges, in: J. Bok, G. Deutscher, D. Pavuna, S.A. Wolf (Eds.), The Gap Symmetry and Fluctuations in High Temperature Superconductors, Plenum Press, 1998, cond-mat/9901333.
[13] J.M. Tranquada, in: Proc. SPIE 5932, 59320C, 2005, cond-mat/0508272;
J.M. Tranquada, in: J.R. Schrieffer (Ed.), Treatise of High Temperature Superconductivity, cond-mat/0512115.
[14] For a review, see M. Eschrig, Adv. Phys. 55 (2006) 47 and references therein.
[15] S.W. Lovesey, Theory of Neutron Scattering from Condensed Matter, vol. 2, Clarendon, Oxford, 1984.
[16] S. Shamoto, M. Sato, J.M. Tranquada, B. Sternlieb, G. Shirane, Phys. Rev. B 48 (1993) 13817.
[17] J. Rossat-Mignod, L.P. Regnault, C. Vettier, P. Bourges, P. Burlet, J. Bossy, et al., Physica C 185–189 (1991) 86.
[18] H.A. Mook, M. Yethiraj, G. Aeppli, T.E. Mason, T. Armstrong, Phys. Rev. Lett. 70 (1993) 3490.
[19] H.F. Fong, B. Keimer, P.W. Anderson, et al., Phys. Rev. Lett. 75 (1995) 316;
H.F. Fong, B. Keimer, P.W. Anderson, et al., Phys. Rev. B 54 (1996) 6708.
[20] P. Bourges, L.P. Regnault, Y. Sidis, C. Vettier, Phys. Rev. B 53 (1996) 876.
[21] H. He, P. Bourges, Y. Sidis, C. Ulrich, L.P. Regnault, S. Pailhès, N.S. Berzigiarova, N.N. Kolesnikov, B. Keimer, Science 295 (2002) 1045.
[22] Y. Sidis, P. Bourges, H.F. Fong, B. Keimer, L.P. Regnault, J. Bossy, A. Ivanov, B. Hennion, P. Gautier-Picard, G. Collin, D.L. Millius, I.A. Aksay, Phys. Rev. Lett. 86 (2001) 4100.
[23] H.F. Fong, P. Bourges, Y. Sidis, L.P. Regnault, A.S. Ivanov, G.D. Gu, N. Koshizuka, B. Keimer, Nature 398 (1999) 588.
[24] S. Pailhès, Y. Sidis, P. Bourges, C. Ulrich, V. Hinkov, L.P. Regnault, A. Ivanov, C. Bernhard, B. Liang, C.T. Lin, B. Keimer, Phys. Rev. Lett. 91 (2003) 237002.
[25] S. Pailhès, Y. Sidis, P. Bourges, V. Hinkov, A. Ivanov, C. Ulrich, L.P. Regnault, B. Keimer, Phys. Rev. Lett. 93 (2004) 167001.
[26] S. Pailhès, C. Ulrich, B. Fauqué, V. Hinkov, Y. Sidis, A. Ivanov, C.T. Lin, B. Keimer, P. Bourges, Phys. Rev. Lett. 96 (2006) 257001.
[27] L. Capogna, B. Fauqué, Y. Sidis, C. Ulrich, P. Bourges, S. Pailhès, A. Ivanov, J.L. Tallon, B. Liang, C.T. Lin, A.I. Rykov, B. Keimer, Phys. Rev. B 75 (2007) 060502.
[28] P. Dai, H.A. Mook, F. Dogan, Phys. Rev. Lett. 80 (1998) 1738.
[29] H.A. Mook, P. Dai, S.M. Hayden, G. Aeppli, T.G. Perring, F. Doğan, Nature 395 (1998) 580.
[30] M. Arai, T. Nishijima, Y. Endoh, T. Egami, S. Tajima, K. Tomimoto, et al., Phys. Rev. Lett. 83 (1999) 608.
[31] H.A. Mook, Pengcheng Dai, F. Dogan, R.D. Hunt, Nature 404 (2000) 729.
[32] P. Bourges, Y. Sidis, H.F. Fong, L.P. Regnault, J. Bossy, A.S. Ivanov, B. Keimer, Science 288 (2000) 1234.
[33] C. Stock, W.J.L. Buyers, R.A. Cowley, P.S. Clegg, R. Coldea, C.D. Frost, R. Liang, D. Peets, D. Bonn, W.N. Hardy, R.J. Birgeneau, Phys. Rev. B 69 (2004) 014502.

[34] D. Reznik, P. Bourges, L. Pintschovius, Y. Endoh, Y. Sidis, T. Masui, S. Tajima, Phys. Rev. Lett. 93 (2004) 207003.
[35] H. Woo, P. Dai, S.M. Hayden, H.A. Mook, T. Dahm, D.J. Scalapino, T.G. Perring, F. Doğan, Nature Phys. 2 (2006) 600.
[36] P. Bourges, H.F. Fong, L.P. Regnault, J. Bossy, C. Vettier, D.L. Milius, I.A. Aksay, B. Keimer, Phys. Rev. B 56 (1997) R11439.
[37] C. Stock, W.J.L. Buyers, R. Liang, D. Peets, Z. Tun, D. Bonn, W.N. Hardy, R.J. Birgeneau, Phys. Rev. B 69 (2004) 014502.
[38] S.M. Hayden, H.A. Mook, Pengcheng Dai, T.G. Perring, F. Doğan, Nature 429 (2004) 531.
[39] V. Hinkov, S. Pailhès, P. Bourges, Y. Sidis, A. Ivanov, A. Kulakov, C.T. Lin, D.P. Chen, C. Bernhard, B. Keimer, Nature 430 (2004) 650.
[40] V. Hinkov, P. Bourges, S. Pailhès, Y. Sidis, A. Ivanov, C.T. Lin, D.P. Chen, B. Keimer, Nature Physics (2007), in press.
[41] F. Onufrieva, P. Pfeuty, cond-mat/9903097.
[42] A. Abanov, A.V. Chubukov, Phys. Rev. Lett. 83 (1999) 1652.
[43] M.N. Norman, Phys. Rev. B 61 (2000) 14751.
[44] D. Manske, I. Eremin, K.H. Bennemann, Phys. Rev. B 63 (2001) 054517.
[45] F. Onufrieva, P. Pfeuty, Phys. Rev. B 65 (2002) 014502, cond-mat/9903097.
[46] J. Brinckmann, P.A. Lee, Phys. Rev. B 65 (2002) 014502.
[47] A.P. Schnyder, A. Bill, C. Mudry, R. Gilardi, H.M. Ronnow, J. Mesot, Phys. Rev. B 70 (2004) 214511.
[48] I. Eremin, D.K. Morr, A.V. Chubukov, K.H. Bennemann, M.R. Norman, Phys. Rev. Lett. 94 (2005) 147001.
[49] S.V. Borisenko, A.A. Kordyuk, V. Zabolotnyy, J. Geck, D. Inosov, A. Koitzsch, J. Fink, M. Knupfer, B. Büchner, V. Hinkov, C.T. Lin, B. Keimer, T. Wolf, S.G. Chiuzbăian, L. Patthey, R. Follath, Phys. Rev. Lett. 96 (2006) 117004, cond-mat/0608295.
[50] B. Fauqué, Y. Sidis, L. Capogna, A. Ivanov, K. Hradil, C. Ulrich, A.I. Rykov, B. Keimer, P. Bourges, cond-mat/0701052.
[51] A. Kordyuk, S.V. Borisenko, M. Knupfer, J. Fink, Phys. Rev. B 67 (2003) 064504;
A.A. Kordyuk, S.V. Borisenko, A. Koitzsch, J. Fink, M. Knupfer, H. Berger, Phys. Rev. B 71 (2005) 214513.
[52] A.J. Millis, H. Monien, Phys. Rev. B 54 (1996) 16172.
[53] T. Li, Z. Gan, Phys. Rev. B 60 (1999) 3092;
T. Li, Phys. Rev. B 64 (2001) 012503.
[54] I. Eremin, D.K. Morr, A.V. Chubukov, K. Bennemann, cond-mat/061267.
[55] T. Zhou, Z.D. Wang, J.-X. Li, cond-mat/0611311.
[56] W.L. McMillan, J.M. Rowell, in: R.D. Parks (Ed.), Superconductivity, Dekker, New York, 1969.
[57] J.C. Campuzano, H. Ding, M.R. Norman, H.M. Fretwell, M. Randeria, A. Kaminski, J. Mesot, T. Takeuchi, T. Sato, T. Yokoya, T. Takahashi, T. Mochiku, K. Kadowaki, P. Guptasarma, D.G. Hinks, Z. Konstantinovic, Z.Z. Li, H. Raffy, Phys. Rev. Lett. 83 (1999) 3709.
[58] J.F. Zasadzinski, L. Ozyuzer, N. Miyakawa, K.E. Gray, D.G. Hinks, C. Kendziora, Phys. Rev. Lett. 87 (2001) 067005.
[59] J. Hwang, T. Timusk, G. Gu, Nature 427 (2004) 714.
[60] S.V. Borisenko, A.A. Kordyuk, A. Koitzsch, J. Fink, J. Geck, V. Zabolotnyy, M. Knupfer, B. Büchner, H. Berger, M. Falub, M. Shi, J. Krempasky, L. Patthey, Phys. Rev. Lett. 96 (2006) 067001.
[61] J.M. Tarascon, P. Barboux, P.F. Miceli, L.H. Greene, G.W. Hull, M. Eibschutz, S.A. Sunshine, Phys. Rev. B 37 (1988) 7458.
[62] P. Mendels, J. Bobroff, G. Collin, H. Alloul, M. Gabay, J.F. Marucco, N. Blanchard, B. Grenier, Europhys. Lett. 46 (1999) 678.
[63] Y. Sidis, P. Bourges, B. Keimer, L.P. Regnault, J. Bossy, A. Ivanov, B. Hennion, P. Gautier-Picard, G. Collin, in: J. Bonca, et al. (Eds.), Open Problems in Strongly Correlated Electron Systems, Kluwer Academic Publisher, 2001, cond-mat/0006265.
[64] H.F. Fong, P. Bourges, Y. Sidis, L.P. Regnault, J. Bossy, A. Ivanov, D.L. Milius, I.A. Aksay, B. Keimer, Phys. Rev. Lett. 82 (1999) 1939.
[65] Y. Sidis, P. Bourges, B. Hennion, L.P. Regnault, R. Villeneuve, G. Collin, J.F. Marucco, Phys. Rev. B 53 (1996) 6811.
[66] V.B. Zabolotnyy, S.V. Borisenko, A.A. Kordyuk, J. Fink, J. Geck, A. Koitzsch, M. Knupfer, B. Büchner, H. Berger, A. Erb, C.T. Lin, B. Keimer, R. Follath, Phys. Rev. Lett. 96 (2006) 037003.
[67] J. Fink, A. Koitzsch, J. Geck, V. Zabolotnyy, M. Knupfer, B. Buchner, A. Chubuckov, H. Berger, cond-mat/0604666.
[68] I. Sega, P. Prelovček, J. Bonča, Phys. Rev. B 68 (2003) 054524.
[69] P. Prelovček, I. Sega, Preprint, cond-mat/0607324.
[70] F. Onufrieva, J. Rossat-Mignot, Phys. Rev. B 52 (1995) 7572.
[71] M.V. Eremin, A.A. Aleev, I.M. Eremin, JETP Lett. 84 (2006) 167.
[72] S.D. Wilson, et al., Nature 42 (2006) 59.
[73] G. Aeppli, T.E. Mason, S.M. Hayden, H.A. Mook, J. Kulda, Science 278 (1997) 1432.
[74] T.E. Mason, A. Schröder, G. Aeppli, H.A. Mook, S.M. Hayden, Phys. Rev. Lett 77 (1996) 1604.
[75] H.F. Fong, P. Bourges, Y. Sidis, L.P. Regnault, J. Bossy, A.S. Ivanov, et al., Phys. Rev. B 61 (2000) 14774.
[76] P. Dai, H.A. Mook, R.D. Hunt, F. Doğan, Phys. Rev. B 63 (2001) 054525.
[77] E.W. Carlson, et al., in: K.H. Bennemann, J.B. Ketterson (Eds.), The Physics of Conventional and Unconventional Superconductors, Springer-Verlag, in press, cond-mat/0206217.
[78] M. Fujita, H. Goka, K. Yamada, J.M. Tranquada, L.P. Regnault, Phys. Rev. B 70 (2004) 104517.
[79] N. Ichikawa, S. Uchida, J.M. Tranquada, T. Niemöller, P.M. Gehring, S.-H. Lee, J.R. Schneider, Phys. Rev. Lett. 85 (2000) 1738.
[80] J.M. Tranquada, H. Woo, T.G. Perring, H. Goka, G.D. Gu, G. Xu, M. Fujita, K. Yamada, Nature 429 (2004) 524.
[81] M. Vojta, T. Ulbricht, Phys. Rev. Lett. 93 (2004) 127002.
[82] G.S. Uhrig, K.P. Schmidt, M. Grüninger, Phys. Rev. Lett. 93 (2004) 267003.
[83] G. Seibold, J. Lorenzana, Phys. Rev. Lett. 94 (2005) 107006.
[84] M. Vojta, T. Vojta, R.K. Kaul, Phys. Rev. Lett. 97 (2006) 097001.
[85] N.B. Christensen, D.F. McMorrow, H.M. Ronnow, B. Lake, S.M. Hayden, G. Aeppli, T.G. Perring, M. Mangkorntong, M. Nohara, H. Tagaki, Phys. Rev. Lett. 93 (2004) 147002.
[86] J. Chang, A.P. Schnyder, R. Gilardi, H.M. Rønnow, S. Pailhes, N.B. Christensen, Ch. Niedermayer, D.F. McMorrow, A. Hiess, A. Stunault, M. Enderle, B. Lake, O. Sobolev, N. Momono, M. Oda, M. Ido, C. Mudry, J. Mesot, Phys. Rev. Lett. 98 (2007) 077004.

[87] F. Kruger, S. Scheidl, Phys. Rev. B 70 (2004) 064421.
[88] J.S. Uhrig, et al., J. Phys. Soc. Japan 74 (Suppl.) (2005) 86.
[89] M.R. Norman, D.P. Pines, C. Kallin, Adv. Phys. 54 (2005) 715, cond-mat/0507031.
[90] M.R. Norman, C. Pépin, Rep. Prog. Phys. 66 (2003) 1547.
[91] T. Timusk, B. Statt, Rep. Prog. Phys. 62 (1999) 61.
[92] Y. Sidis, B. Fauqué, V. Aji, P. Bourges, in: Proceedings of PNCMI Conference, Physica B 397 (1) (2007) 1–6.